Reshaping a multimode laser beam into a constructed Gaussian beam for generating a thin light sheet

Article *in* Journal of Biophotonics · February 2018

DOI: 10.1002/jbio.201700213

CITATIONS
0

READS
137

13 authors, including:

S. Saghafi
TU Wien-Vienna University of Technology
87 PUBLICATIONS **862** CITATIONS
SEE PROFILE

Nikoo Haghi-Danaloo
2 PUBLICATIONS **0** CITATIONS
SEE PROFILE

Klaus Becker
Medical University of Vienna
92 PUBLICATIONS **1,776** CITATIONS
SEE PROFILE

Inna Sabdyusheva
Medical University of Vienna
21 PUBLICATIONS **27** CITATIONS
SEE PROFILE

Received: 6 August 2017 | Accepted: 14 February 2018

DOI: 10.1002/jbio.201700213

Journal of BIOPHOTONICS

FULL ARTICLE

Reshaping a multimode laser beam into a constructed Gaussian beam for generating a thin light sheet

Saiedeh Saghafi[1,2]* | Nikoo Haghi-Danaloo[1] | Klaus Becker[1,2] | Inna Sabdyusheva[1,2] | Massih Foroughipour[1,2] | Christian Hahn[1,2] | Marko Pende[1,2] | Martina Wanis[1,2] | Michael Bergmann[3,4,5] | Judith Stift[3,4,5] | Balazs Hegedus[3,5] | Balazs Dome[3,4,5] | Hans-Ulrich Dodt[1,2]

[1]Department of Bioelectronics, FKE, Vienna University of Technology-TU Wien, Vienna, Austria

[2]Section of Bioelectronics, Center for Brain Research, Medical University of Vienna, Vienna, Austria

[3]Department of Surgery, Medical University of Vienna, Vienna, Austria

[4]Department of Pathology, Medical University of Vienna, Vienna, Austria

[5]Cancer BioBank, Medical University of Vienna, Vienna, Austria

***Correspondence**
Saiedeh Saghafi, Department of Bioelectronics, FKE, Vienna University of Technology-TU Wien, Vienna, Austria.
Email: saiedeh.saghafi@tuwien.ac.at

Funding information
Austrian Science Fund (FWF), Grant/Award number: P23102-N22

Based on the modal analysis method, we developed a model that describes the output beam of a diode-pumped solid state (DPSS) laser emitting a multimode beam. Measuring the output beam profile in the near field and at the constructed far field the individual modes, their respective contributions, and their optical parameters are determined. Using this information, the beam is optically reshaped into a quasi-Gaussian beam by the interference and superposition of the various modes. This process is controlled by a mode modulator unit that includes different meso-aspheric elements and a soft-aperture. The converted beam is guided into a second optical unit comprising achromatic-aspheric elements to produce a thin light sheet for ultramicroscopy. We found that this light sheet is markedly thinner and exhibits less side shoulders compared with a light sheet directly generated from the output of a DPSS multimode laser.

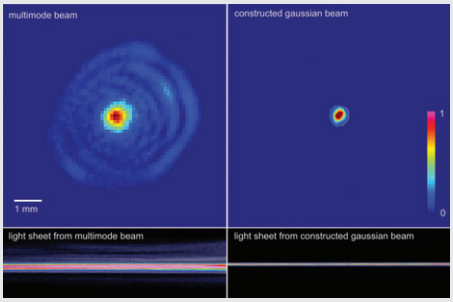

KEYWORDS
multimode laser, constructed gaussian beam, Light sheet microscopy, light sheet generator, laser beam shaping

1 | INTRODUCTION

The nature of light as an electromagnetic wave suggests that the solutions of the Maxwell's equations can be used to describe beam propagation. Maxwell's equations can be reduced to a simpler form (wave equations) and be written in terms of either the electric or the magnetic field. Using these wave equations, the complex vector function describing an optical field can be developed into an asymptotic series approximation called ray series. Due to the computational difficulties, the higher order terms of the ray expansion usually are not used. However, the zero order of the ray series provides a satisfactory analysis for many problems in physical applications. Here, we perform an optical characterization of the output beam of a commercially available multimode laser, which shows that modal

analysis provides intuitive explanations about the modal structure of transversal modes along the *x*-*y* plane normal to the *z*-axis, the beam intensity, the beam width and the phase, at any arbitrary point.

2 | MATERIALS AND METHODS

2.1 | Theory

The optical field can be characterized using the theory of wave optics (physical optics). Recalling the Huygens' Principle, an arbitrary incoherent source is described as the incoherent superposition of independent spherical waves. The solutions of the familiar wave equation provide adequate information about the beam phase and amplitude at any point. The scalar wave equation can be written as $\nabla^2\psi(r, t) = \varepsilon\mu\partial^2\psi(r, t)/\partial t^2$, where ε and μ are the permittivity and the permeability of the medium. In physical optics, the exact solution of the wave equations (eg, Helmholtz equation), is generally impractical, thus approximations are used; the paraxial approximation applies when the beam waist is large relative to the wavelength and the angle of divergence is small.

The multipole expansion method provides solutions to the wave equation. Any solution of Maxwell's equation can be expressed as the summation of incoming and outgoing electric and magnetic multipole fields. *The superposition of any 2 solutions is also a solution, and this is referred to as the principle of superposition* [1]. The electromagnetic field at a point *far from a focus* is described by expansion of the diffraction integral into a series of functions such as Gegenbauer polynomials or spherical Bessel functions [2]. This method has been used to investigate the effects of different amplitude weighting and can be extended to truncated Gaussian beams or systems with spherical aberration.

Defining an arbitrary field as the modal superposition of individual fields, and employing the angular spectrum method (Fourier optics) in the framework of wave optics can provide accurate results for the propagation of each component. The field characteristics can be described by a superposition of the propagated components. Using the current solutions of the paraxial wave equation enables to describe the propagation of an arbitrary laser beam from near- to far-field.

2.1.1 | Angular spectrum

If a field is Fourier analyzed, its amplitude at any arbitrary point can be calculated by the superposition of its Fourier components, expressed as a plane wave traveling in different directions. This method is called the angular spectrum method and the field expressed by $\psi(x, y, 0)$, is given by the Fourier transform [3]:

$$A_0(f_x,f_y) = \int\int \psi(x,y,0)\exp\left[-2\pi i\left(f_x x + f_y y\right)\right]dxdy. \quad (1)$$

where f_x and f_y are the rectangular coordinates of the Fourier components.

Of course $\psi(x, y, 0)$ can be written as the inverse transform of $A_0(f_x,f_y)$:

$$\psi(x,y,0) = \int\int A_0\left(f_x,f_y\right)\exp\left[2\pi i\left(f_x x + f_y y\right)\right]df_x df_y. \quad (2)$$

Thus, any arbitrary plane wave with unit amplitude that propagates with direction cosines (*L*, *M*, *N*), at any point is given by:

$$\psi(x,y,z) = \int\int A_0\left(\frac{L}{\lambda},\frac{M}{\lambda}\right)\exp\left[2\pi i\left(\frac{L}{\lambda}x + \frac{M}{\lambda}y\right)\right] \times \exp\left[2\pi i\frac{N}{\lambda}z\right]d\left(\frac{L}{\lambda}\right)d\left(\frac{M}{\lambda}\right), \quad (3)$$

where $N = \sqrt{1-L^2-M^2}$, $f_x = \frac{L}{\lambda}$ and $f_y = \frac{M}{\lambda}$.

By defining the modal structure of any arbitrary field, Eq. (3) allows us to obtain the field distribution at any plane.

2.1.2 | Transversal modes analysis

The amplitude of a complex scalar field $\psi(x,y,z)$ satisfying the reduced-wave equation:

$$\left(\nabla^2 + k^2\right)\psi(x,y,z) = 0, \quad (4)$$

and the term $\exp(-i\omega t)$ (phase) together represent the wave field. The most fundamental mode (TEM_{00} mode) is described by a Gaussian function. At $z = 0$ it can be described by:

$$\psi(x,y,0) = \psi_0\exp\left(-k\left(x^2+y^2\right)/2a\right). \quad (5)$$

The parameter a, and the wave number k are real constants and related through $a = kw_0^2$, where w_0 is the beam spot-size. Using the angular spectrum, the field distribution at any arbitrary point is given by Eq. (6):

$$\psi(x;z) = \psi_0 w_0\sqrt{2\pi}\sqrt{\frac{2\pi w_0^2 - i\lambda z}{\left(2\pi w_0^2\right)^2 + \left(\lambda z\right)^2}}\exp[ikz] \times \exp\left[\frac{i\frac{\lambda z}{\pi}x^2}{w_0^4 + \left(\frac{\lambda z}{\pi}\right)^2}\right]\exp\left[\frac{-x^2}{w_0^4 + \left(\frac{\lambda z}{\pi w_0}\right)^2}\right]. \quad (6)$$

The rapid phase variation due to the traveling-wave part of propagation, the wavefront curvature, and the amplitude of the transverse profile are given as $\exp[ikz]$, $\exp\left[\frac{i\lambda z}{\pi}\frac{x^2}{w_0^4+\left(\frac{\lambda z}{\pi}\right)^2}\right]$ and $\exp\left[-\frac{x^2}{w_0^4+\left(\frac{\lambda z}{\pi w_0}\right)^2}\right]$, respectively. The details can be found in Appendix S1, Supporting Information.

However, there are lasers that do not operate in the fundamental mode and their beam profiles are more complex.

Employing higher-order solutions of the paraxial wave equation can be helpful to describe multimode beams.

A combination of Hermite and Gaussian components in rectangular coordinates, or Laguerre and Gaussian components for cylindrical coordinates that are Eigen modes of the paraxial wave equation, can be used as a helpful tool to partially describe multimode beams.

In the standard form of a higher order solution, where the paraxial approximation is applied, the Gaussian part has a complex argument, while the Hermite or Laguerre part has a purely real argument [4]. The field distribution of standard Laguerre-Gaussian modes along the propagation axis is given by:

$$\psi_{mn}(r,\theta,z)=\sqrt{\frac{2m!}{(1+\delta_{0n})\pi(m+n)!}}\frac{\exp[-i(2m+n+1)(\varphi(z)-\varphi_0)]}{w(z)}\times\left(\frac{\sqrt{2}r}{w(z)}\right)^n L_m^n\left(\frac{2r^2}{w^2(z)}\right)\exp\left[ik\frac{r^2}{2q(z)}+in\theta\right] \quad (7)$$

where m, n and L_m^n are the radial index, the azimuthal mode index and a generalized Laguerre polynomial, respectively. The phase shift (the difference between the phase at the observation point and at the waist, $z = 0$) is defined as $(\varphi(z) - \varphi_0)$. This, together with $(2\ m + n + 1)$ yields the Gouy phase shift factor. The variation along the azimuthal direction is $\exp(in\theta)$. The beam spot size and the complex radius of curvature are described by

$w(z)=w_0\sqrt{1+(z/z_R)^2}$ (ie, $z_R^2=\left(\pi w_0^2/\lambda\right)^2$), and $q(z)=\pi w_0^2/i\lambda+z$.

This can be easily extended into rectangular coordinates.

However, in cases involving more phase variation other biorthogonal solutions are required that *are not orthogonal in the usual sense*, the so-called elegant modes. They have the same complex scaling factor in the argument of both the Gaussian part as well as the polynomial function [4]. In the near- and in the far-field, the field distribution is described by Eq. (8):

$$\psi_{mn}(r,\theta,0)=\left(\tfrac{r}{w_0}\right)^n L_m^n\left(\frac{r^2}{w_0^2}\right)\exp\left[-\frac{r^2}{w_0^2}+in\theta\right]$$

$$\hat{\psi}(\eta,\theta,z)=\left(\frac{i^{2m+n-1}kw_0^2}{z}\right)\exp\left[ik\left(z+\frac{\eta^2}{2z}\right)\right](2)^{-(n+1)}\left(-\frac{kw_0\eta}{z}\right)^n\times\exp\left(-\left(\frac{kw_0\eta}{2z}\right)^2\right)L_m^{m+n}\left(\left(\frac{kw_0\eta}{2z}\right)^2\right)e^{in\theta} \quad (8)$$

where r and η are the cylindrical coordinates in the near and far field and the rest of the functions and parameters are as described before. Furthermore, mode converters can act like a bridge between standard higher order modes and twisted modes with a complex argument [5]. For many laser applications, a beam with a uniform intensity profile (ie, uniform energy density over a defined cross section) is crucial. For example, the needs of many high-power visible laser applications (eg. micro-machining) are best met by laser sources that have both flat top intensity profiles (uniform energy density over a given cross section) and high beam quality (low divergence output). There are models that were developed based on the number of beam orders in a finite sum of Laguerre-Gaussian functions [6], [7]. They provide analytical expressions in cylindrical coordinates to describe a beam with a uniform profile. The Flattened Gaussian Beam (FGB) describing an axially symmetric uniform beam is given by [6].

$$\psi_N(r,z)\approx\frac{w_N(0)}{w_N(z)}\exp\left[i\left(kz-\Phi_N(z)+\frac{k}{2R_N(z)}\right)\right]\times\exp\left[-\frac{r^2}{w_N^2(z)}\right]\sum_{n=0}^{N}C_n^N L_n\left[\frac{2r^2}{w_N^2(z)}\right]\exp[-2in\Phi_N(z)] \quad (9)$$

where k (the wave number), $w_N(z)$ (the beam spot size at z), $R_N(z)$ (the radius of the curvature), $\phi_N(z)$ (the phase shift) and $w_N(0)$ (the spot size of the Laguerre-Gaussian function at $z = 0$) are sequentially formulated as:

$$k=\tfrac{2\pi}{\lambda},\ w_N(z)=w_N(0)\sqrt{1+\left[\tfrac{\lambda z}{\pi w_N^2(0)}\right]^2},\ R_N(z)=z(1+\left[\tfrac{\pi w_N^2(0)}{\lambda z}\right]^2),\ \Phi_N(z)=\arctan\left[\tfrac{\lambda z}{\pi w_N^2(0)}\right]\text{ and }w_N(0)=\tfrac{w_0}{\sqrt{N}}.$$

Many commercial lasers, the so-called multimode lasers, have particular transversal beam profiles that cannot be solely described by either of the models mentioned above. In this paper, we will approximate the output beam profile of our multimode laser as an incoherent sum of the beam distribution generated by different beam modes (ie, the fundamental and higher order modes), which will be discussed in details later.

As we use lasers as an excitation source for the fluorochromes of cleared biological samples, our methods of histological sample preparation for microscopy are described in the following section.

2.2 | Experimental procedures related to imaging of biological samples by ultramicroscopy

2.2.1 | Chemical clearing of cancer tissue

Cancer tissue of about 1 cm^3 size, fixated with 4% paraformaldehyde was obtained from the Cancer BioBank of the Medical University of Vienna (ethics permission number: #1580/2017). The samples were dehydrated in an ascending aqueous concentration series of tetrahydrofuran (THF, Sigma-Aldrich, Austria, 50%, 80%, 96%, 100%, 1 to 2 hours per step, last step overnight). Afterward, they were immersed in dibenzyl ether (DBE) for refractive index matching until they became transparent (3-6 weeks) [8].

2.2.2 | Chemical clearing of Drosophila flies

Drosophila flies were fixated in 4% formaldehyde and then dehydrated in an ascending concentration series of 30, 50, 70, 80, 90, 96 and 3x100% THF (Sigma-Aldrich).

Afterward, they were immersed in DBE (Sigma-Aldrich) for 2 hours to render them transparent. For storage, the DBE was replaced by fresh clearing solution [8].

2.2.3 | Preparation and chemical clearing of mouse brains

Mouse brains were obtained from a thy-1 YFP (yellow fluorescent protein) expressing mouse line [9]. The mice were killed using CO_2 gas, transcardially perfused postmortem with phosphate buffered saline (PBS), and fixed with 4% formaldehyde in PBS. After preparation, the brains were dehydrated in ascending concentration series of peroxide free THF, and incubated in peroxide-free DBE until they became transparent. Animal care and euthanasia was done in accordance with the ethics guidelines of the Austrian animal protection law.

3 | RESULTS

3.1 | Multimode beam analysis

In this paper, based on the current solutions of the paraxial wave equation, a parametric description is developed that describes the beam propagation of a number of multimode lasers including the output beam of a multimode diode-pumped solid state (DPSS) laser emitting a 540 nm beam. This type of laser is widely used in various scientific fields such as food industry, life sciences and particularly in microscopy [8]. In light sheet microscopy it is known that the quality of the images is highly dependent upon the properties of the laser beam profile.

Using modal analysis, we developed a general description that approximates the output beam distribution of a multimode laser beam through the incoherent sum of beam profiles generated by different beam modes as given by Eq. (10):

$$I = a\left[\left[A_1 \exp\left[-\frac{2Nr^2}{w_1^2(z)}\right]\right]\left\{\left(\sum_{p=0}^{N} C_p^N L_p\left[\frac{2(N)r^2}{w_1^2(z)}\right]\right.\right.$$

$$\left.\times \cos\left[2n\Phi_N(z)\right]\right)^2 + \left(\sum_{p=0}^{N} C_p^N L_p\left[\frac{2Nr^2}{w_1^2(z)}\right] \sin\left[2n\Phi_N(z)\right]\right)^2\Bigg\}\Bigg]$$

$$+ b\left[A_2 \exp\left(-\frac{2r^2}{w_2(z)^2}\right)\right] + c\left[A_3\left(\frac{\sqrt{2}r}{w_3(z)}\right)^n L_m^n\left(\frac{2r^2}{w_3(z)^2}\right)\right.$$

$$\left.\times \exp\left[-\frac{r^2}{w_3(z)^2}\right]\right]^2 + d\left[A_4\left(\frac{\sqrt{2}r}{w_4(z)}\right)^{n1} L_{m1}^{n1}\left(\frac{2r^2}{w_4(z)^2}\right)\right.$$

$$\left.\times \exp\left[-\frac{r^2}{w_4(z)^2}\right]\right]^2 \qquad (10)$$

where a, b, c and d are mode contribution factors, and A_1, A_2, A_3 and A_4 are amplitude normalization parameters. $w_1(z)$, $w_2(z)$, $w_3(z)$ and $w_4(z)$ are the beam spot-sizes of a flat-top beam, a Gaussian beam, and 2 different Laguerre Gaussian beams at any arbitrary point along the propagation axis. Furthermore, L_p, L_m^n, L_{m1}^{n1}, are Laguerre polynomials of order p, generalized Laguerre polynomials of the orders (m, n) and (m_1, n_1). r and θ are the cylindrical transversal coordinates. The parameters m and n are azimuthal and radial mode indices. C_p^N is given by $C_p^N = (-1)^p \sum_{m=p}^{N} \binom{m}{n} \frac{1}{2^m}$.

Figure 1 shows beam profiles in the near-field and in the far-field simulated according to Eq. (10) using 2 different sets of parameters.

3.2 | Experimental analysis

For our experiments we employed a DPSS laser (MGL-540, $M^2 < 2$, China) that emits multimode beam at ~540 nm with 100 mW effective power. Using a LaserCam-HRTM II (2/3-inch) beam analyzer with a sensor element of 1280*1024 pixels/sensor active area 8.3 mm*6.6 mm (Coherent Inc., Germany), the beam profiles in the near-field and in the far-field were measured as shown in Figure 2A,B.

A custom-made program was developed that fits the parameters from Eq. (10) to measure beam-intensity profiles. The program utilizes the DIRECT algorithm [10] from the TOMLAB optimization toolbox (TOMLAB software AB, Sweden) to find matching values for the integer parameters p, q, p_1 and q_1 and the *fmincon* solver provided by the MATLAB optimization toolbox (MathWorks, Germany) as a sub-solver to find best parameter values for the model parameters a, b, c, d and w_{01}, w_{02}, w_{03}, w_{04}. Best congruence between model prediction and measured data was defined as:

$$\min\left(\sum_{i=1}^{n}\left(I_{i,m} - I_{i,p}(a,b,c,d,w_{01},w_{02},w_{03},w_{04})\right)^2\right) \qquad (11)$$

$I_{i,\mathrm{m}}$: measured intensity at point i, $I_{i,p}$: predicted intensity at point i according to Eq. (10), n: number of measured intensity values. N was pinned to a constant value of 10, yielding a sufficient compromise between numerical precision and computation speed.

The fitting routine provides values for the parameters describing the beam width of the maximum peak as well as the other contributor modes, the number of rings, and the steepness of the maximum peak related to N as shown in Figure 2C,D.

3.3 | Laser mode modulator and light sheet generator

Recognizing the modes and their contributions in the profile is the initial step toward creating a beam with improved quality. We developed a patented mode modulator (MM) unit containing meso-aspheric elements in combination with a custom-made soft-aperture to reshape a multimode beam into a constructed Gaussian beam. The

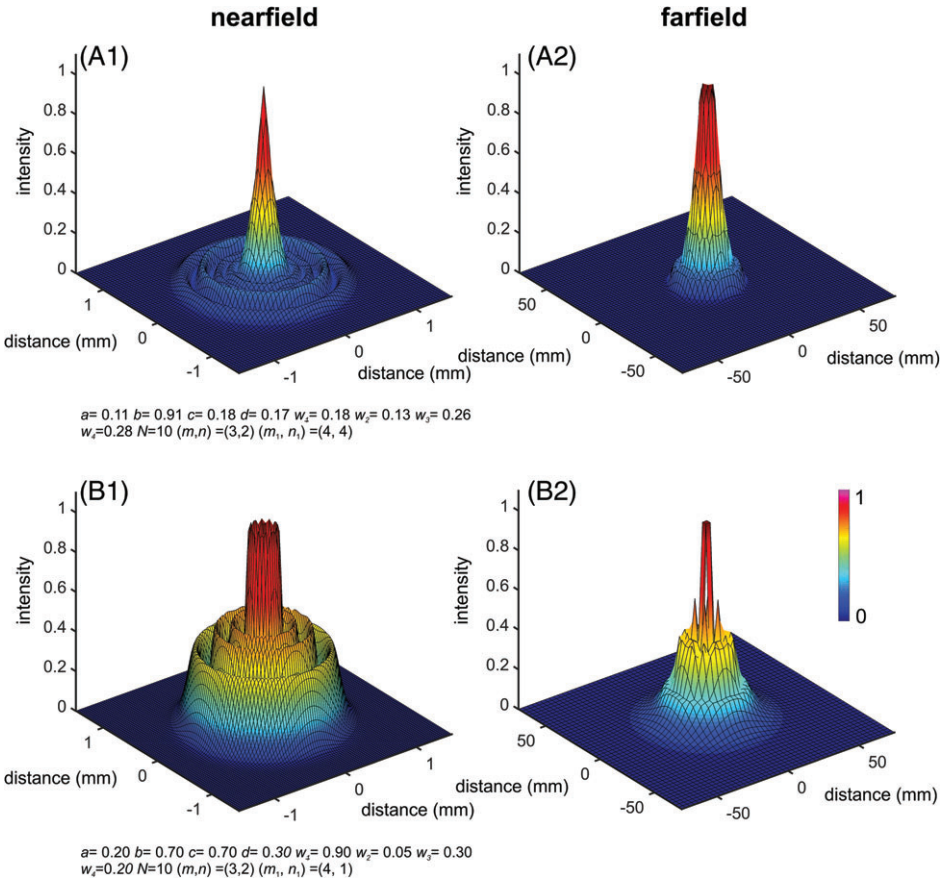

FIGURE 1 Three dimensional beam-intensity profiles simulated according to Eq. (10) in the near-field (A1, B1) and in the far-field (A2, B2) using 2 different parameter sets

modulator subdues the higher order modes that have the least contribution in the power and enforces other modes to encounter optical phenomena such as partially diffraction, interference and superposition to create a constructed Gaussian beam.

We divided the output beam of our DPSS multimode laser by a 50% beam splitter and guided both beams toward 2 identical MM-units containing several elements with particular surface structure. These 2 units are connected to 2 adjoined patented light sheet generators (LSGs) that were

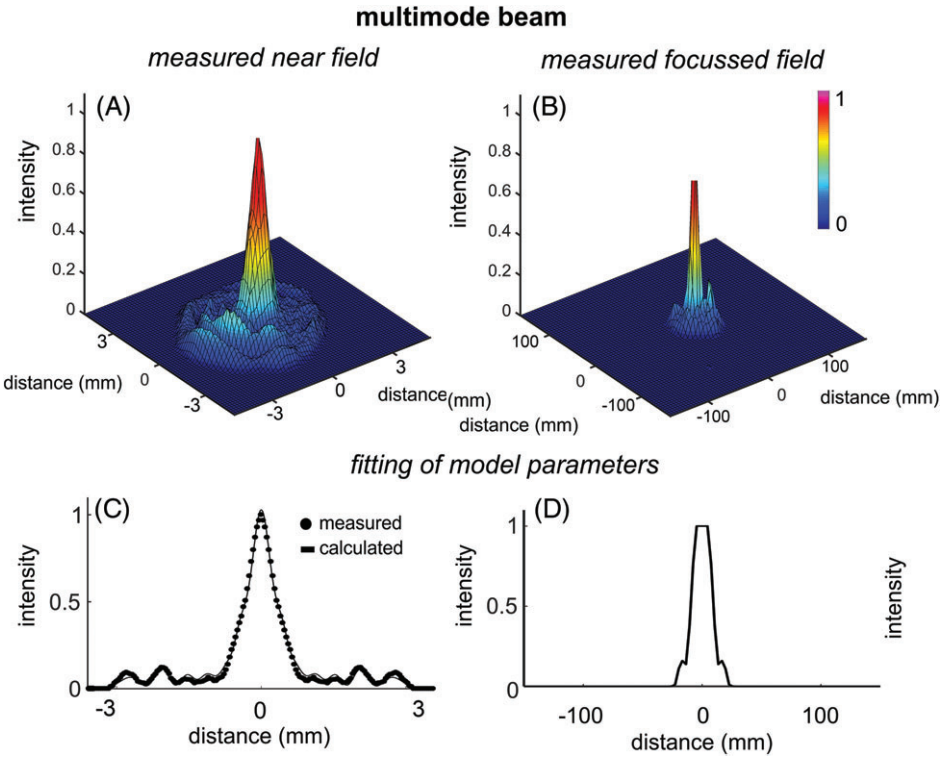

FIGURE 2 Optical characterization of a multimode DPSS laser. A, 3D beam-intensity profiles of the multimode DPSS laser in the near-field. The maximum beam spot-size is ~3.4 mm at $z = 0$ and at 50 cm away from the laser it becomes ~5.8 mm. B, 3D beam-intensity profiles of the multimode DPSS laser at the constructed far-field using a converging lens. C, The comparison of measured data and simulated intensity profiles using extracted values of $a = 0.11$, $b = 0.91$, $c = 0.18$, $d = 0.17$, $w_1(z = 0) = 0.18$ mm, $w_2(z = 0) = 0.13$ mm, $w_3(z = 0) = 0.26$ mm, $w_4(z = 0) = 0.28$ mm, $N = 10$, $(m, n) = (3; 2)$, $(m_1, n_1) = (4; 4)$ employing Eq. (10). D, The simulated profiles at the far-field using the extracted parameters

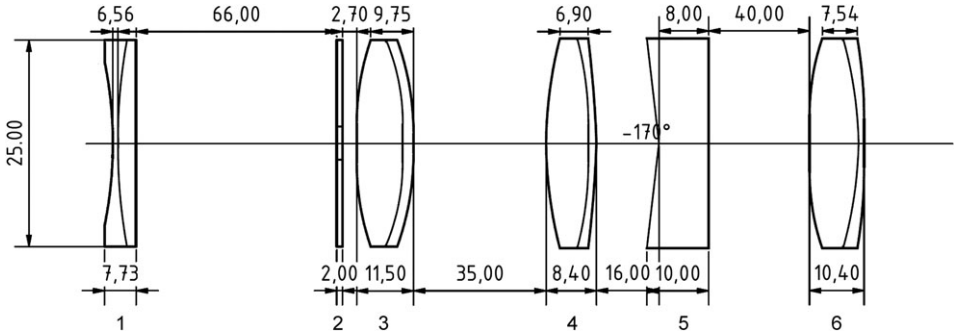

FIGURE 3 Optical design of the *multimode beam modulator* (MM). Schematic optical drawing of the MM. By passing through the MM the output beam of the multimode laser (540 nm/100 mW) is converted into a quasi-Gaussian beam. (1) A negative achromatic lens with a focal length of 150 mm (Edmund Optics, Germany). (2) A custom-made soft aperture. (3) An aspherized achromatic positive lens of focal length +50 mm (Edmund Optics, Germany). (4) An achromatic positive lens of 125 mm (Edmund Optics, Germany), (5) A plano-concave conic lens of fan-angle −170° (Stands Ltd, Lithunia). (6) An aspherized achromatic lens of focal length 40 mm (Edmund Optics, Germany)

built according to a design published in 2014 [11]. They are placed on alternate sides of a quartz chamber containing the biological samples for light sheet microscopy.

Most DPSS lasers emitting multimode beam have a semiuniform central peak surrounded by few rings. If the contributions of the energy in the outer rings are not substantial, we can cut them off using and annular aperture and generate a beam that seems Gaussian at a quick glance over a limited distance; however, this beam will expand rapidly and is not useable. Furthermore, if the standard parameters such as M^2 and the kurtosis factor that demonstrate the similarities of an arbitrary beam to a diffraction limited beam are considered, we will see that those truncated beams are far from the standard Gaussian beam [12, 13]. Those truncated beams may not contain many outer rings, but the flatness, steepness of the side shoulder and various properties related to different modes remain intact.

Based on the modes that approximate our beam, we used the Zemax software to simulate the effects of various optical elements on the beam. The optical elements were chosen in a way to eliminate the unwanted rings while conserving the energy.

The first optical element in each of the 2 MM-units (the furthest lens from the LSG unit) is a negative achromatic lens with a focal length of 150 mm (Edmund Optics, Germany). It expands the beam in order to allow the soft aperture to eliminate the furthest ring without disturbing the main structure that contains most of the energy. This is done

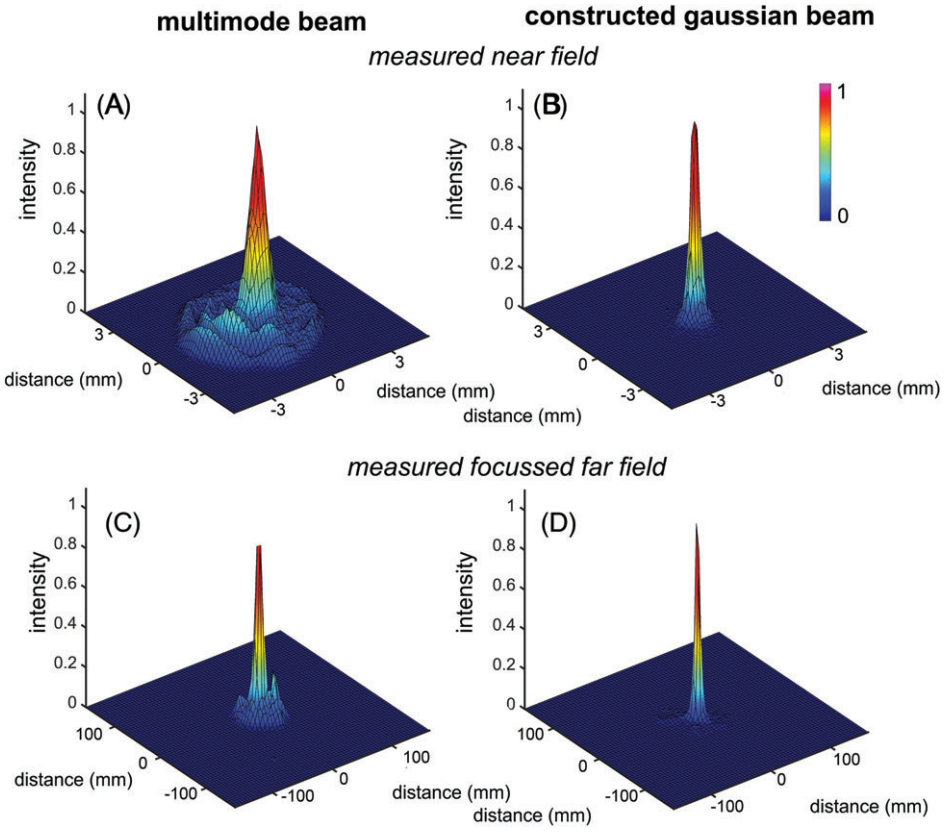

FIGURE 4 Comparison of the multimode beam profile with and without mode modulator (MM). A, 3D intensity distribution of the multimode beam generated by the DPSS laser in the near-field. B, 3D intensity distribution of the constructed Gaussian beam in the near-field. C, 3D intensity profile of multimode bean at the far-field. D, 3D beam profile of the constructed Gaussian at the far-field

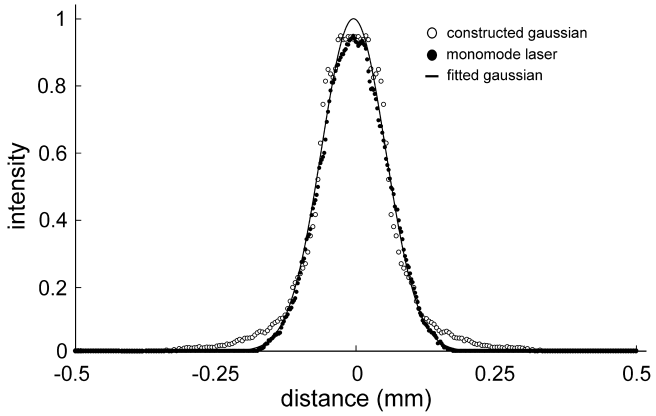

FIGURE 5 A comparison between the output beam profile of the constructed Gaussian beam, the output beam of a monomode laser (Coherent Inc., Germany/200 mW, 532 nm) and an ideal Gaussian beam

due to the density variation of a gradient coating around the center of the filter. A commercial Bulleyes filter can be used; however, it may eliminate even desirable light. In addition, it is directly related to the required beam size of the fourth element, which is a plano-concave conic lens. The third optical element is an aspherized achromatic positive lens of focal length +50 mm (Edmund Optics, Germany). The fourth is an achromatic positive lens of 125 mm (Edmund Optics, Germany), which in conjunction with the 2 first lenses generates a parallel beam that is incident on a plano-concave conic lens of fan-angle −170° (Stands Ltd, Lithuania). Due to the structure of this conic element, the various modes undergo specific changes. This alteration is intensified by the last aspherized achromatic lens of focal length 40 mm (Edmund Optics, Germany), producing a beam with constructed Gaussian mode.

This beam profile is checked over a distance of 1500 mm by a LaserCam-HRTM II (Coherent Inc.) demonstrating a Gaussian profile with M^2~1.2. The free propagation of the beam over 30 000 mm demonstrates that it remains Gaussian and the coherency is comparable with a monomode laser beam (Videos S1 – S3). The schematic of the design is shown in Figure 3.

Figure 4 demonstrates a comparison between the original laser beam and the constructed Gaussian beam in near- and far-field. While the original multimode beam expectedly exhibits numerous side shoulders (Figure 2A), the beam quality achieved after sending the beam through the MM-unit comes close to the output of a much more expensive single mode Sapphire laser (Coherent Inc.) emitting 532 nm/200 mW green beam (Figure 5). Furthermore, the constructed Gaussian beam generated by the MM-unit is preserved up to 70% of the initial power.

The light sheet generated by the described MM-unit in conjunction with the LSG [11] as shown in Figure 6A1 is used for ultramicroscopy (Video S4). Figure 6A2,A3 shows a comparison of the light sheet that is generated from the multimode DPSS laser output beam directly incident to the LSG with the light sheet that is generated if the laser beam is first sent through the MM-unit.

The light sheet, for both multimode beam and the constructed Gaussian beam was recorded at the particular

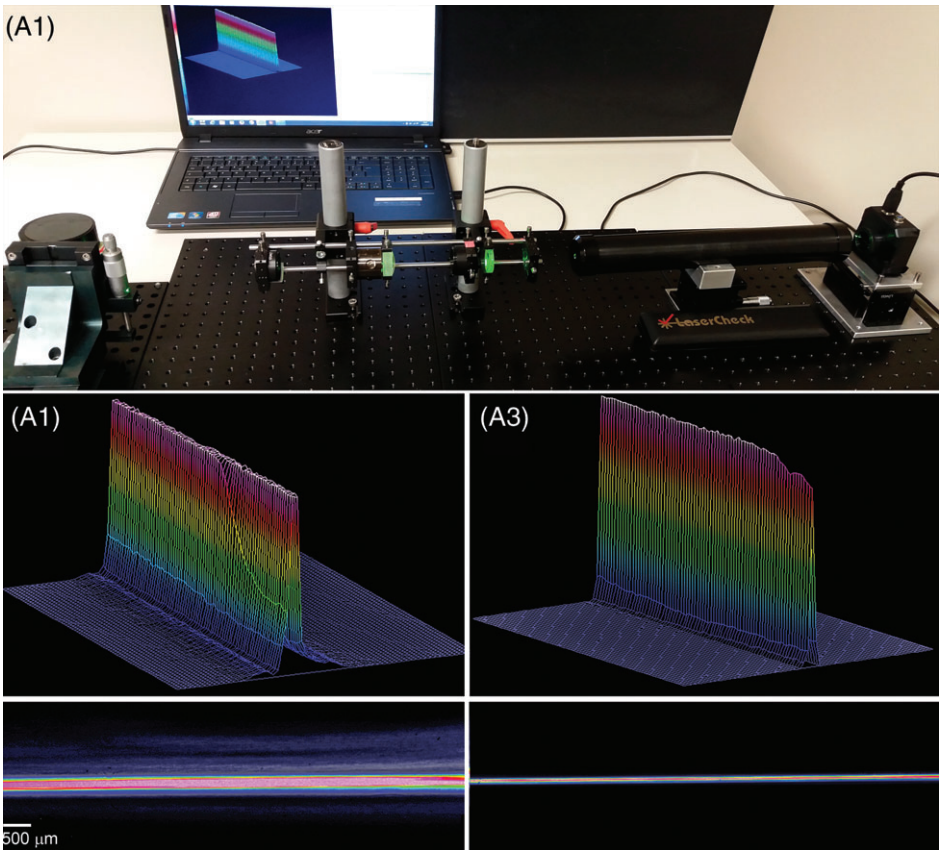

FIGURE 6 Light sheet produced by light generator-LSG unit with and without the mode modulator (MM). A1, DPSS Laser/MMA/LSG/a LaserCam-HRTM II (Coherent Inc., Germany). A2, Light sheet generated by sending the laser beam through the LSG without MM. A3, Light sheet generated by sending the laser beam through the LSG with MM. It is clear that the quality of the light sheet generated by the modulated beam has improved markedly

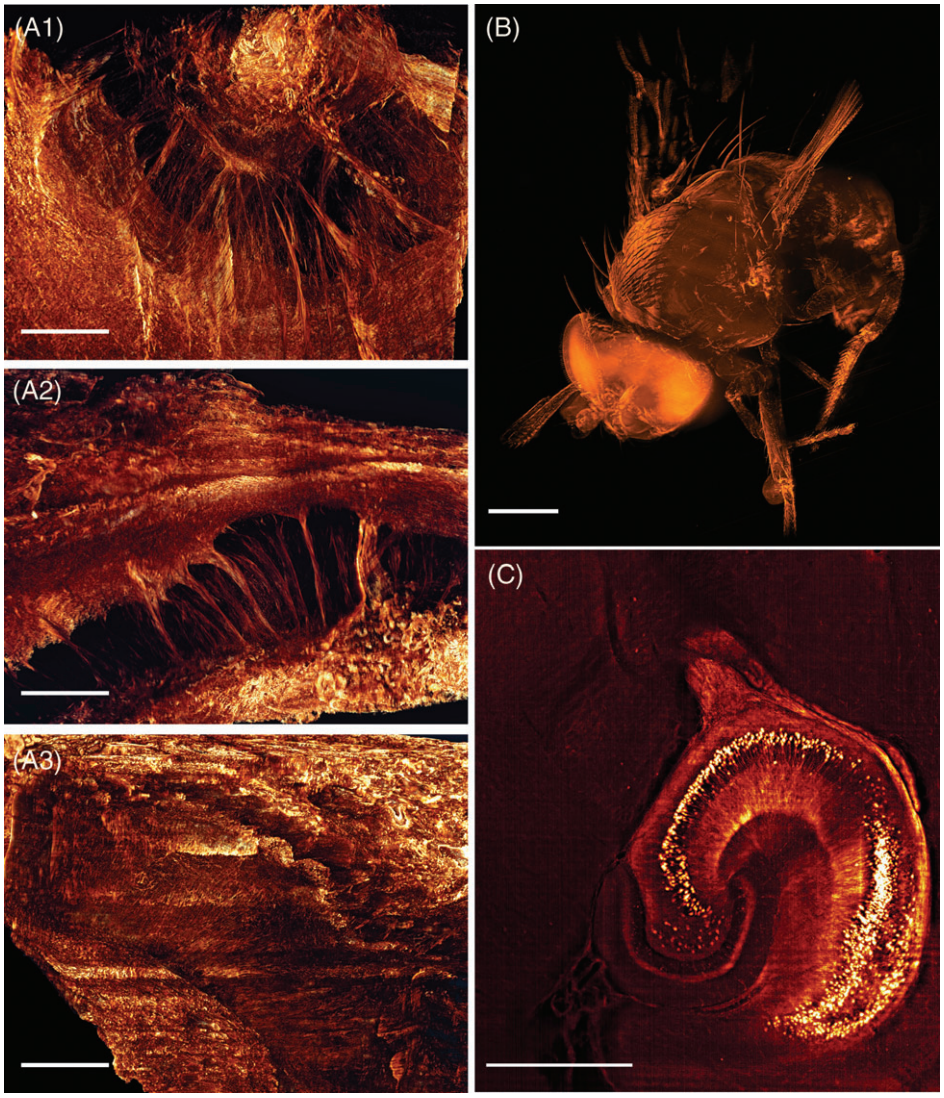

FIGURE 7 (A1-A3) 3D reconstructions of cleared biological samples. All application examples were obtained using the light sheet generator described in this paper and a ×4 objective corrected for a refractive index of 1.56. Fluorescence excitation was induced by laser light of 540 nm wavelength. (A1-A3) 3D-reconstruction from a chemically cleared tissue block of human colon cancer, size 10 mm × 10 mm × 10 mm, image width 4 mm. Reconstruction was obtained from 1500 optical sections. View A1 (*xy*) corresponds to the recording plane. A2 and A3 are calculated views from orthogonal directions (*xz* and *yz*, respectively). As can be seen by the view from all 3 spatial directions resolution is almost isotropic. Length of scale bar: 1000 µm. (B) 3D-reconstruction of a cleared fly (*Drosophila melanogaster*) using its autofluorescene. Length of scale bar: 500 µm. (C) View into of a cleared mouse brain showing parts of its GFP labeled hippocampal formation by reconstruction form 150 optical sections. Length of scale bar: 500 µm

position when the light sheet has a minimum beam-width. The full-width-half-maximum (FWHM) of the light sheet generated by the constructed Gaussian incident on the LSG unit is ~4.0 µm while the one produced by the multimode beam is ~18 µm. At 5 mm away, the width of the light sheet produced by the constructed Gaussian becomes ~75 µm while the one produced by a multimode beam reaches to 382 µm.

It is obvious from the 3D plot of the beam profile that the light sheet generated from the constructed Gaussian beam is much thinner and almost free from any side shoulders.

The LSG is mounted in a tube and placed on a computer-controlled linear stage (LS-65, PI-Micos, Germany) that can be moved along the beam propagation axis for shifting the optimal line of focus. The chemically cleared specimens are placed inside of a quartz chamber filled with a clearing solution of the same refractive index as the sample. Using this setup the specimen is vertically scanned by the light sheet in small steps on the micrometer scale [14].

Chemically cleared samples emit light, when they are excited by light of 540 nm wavelength. We used this autofluorescence to generate image stacks of different biological samples. Imaging was done using a detecting unit comprising modified objectives that were designed to compensate the refractive index mismatch between air and immersion liquid, an optical band-pass filter, a standard Olympus tube lens and a scientific grade camera (Andor Neo/sCMOS, 2560*2106 pixels, Andor, UK). From the recorded stacks, 3D reconstructions were generated using the software Amira 6.3 (FEI, France). Figure 7 shows 3D reconstructions from different chemically cleared samples as human colon cancer tissue (video S5), a drosophila fly and a green fluorescent protein (GFP) expressing mouse brain. As obvious from Figure 7A1-A3 the obtained resolution is virtually isotropic in all 3 spatial directions.

4 | DISCUSSION AND SUMMARY

We used the modal analysis method for multimode beam diagnosis of a laser beam generated by a DPSS laser. Based on the modes contributions in the output beam profile, we designed a multimode beam modulator that subdues the higher order modes by constructive interference to generate

a quasi-Gaussian beam. This beam is not an ideal Gaussian. According to the International Standard Organization, we can obtain values for 2 quantifying parameters that demonstrate how far our beam deviates from an ideal Gaussian beam. These 2 parameters are the M^2 (beam propagation factor) and the *k-factor* (Kurtosis parameter) [12], [13]. They are given by Eqs. (11) and (12) and have values of 1 and 3, respectively, for an ideal TEM_{00} mode.

$$M^2 = \frac{\sqrt{\left(\int_{-\infty}^{\infty} |\psi(x,z)|^2 x^2 dx\right)\left(\int_{-\infty}^{\infty} \left|\frac{d\psi(x,z)}{dx}\right|^2 dx\right)}}{\left(\int_{-\infty}^{\infty} |\psi(x,z)|^2 dx\right)^2} \quad (11)$$

$$k(z) = \frac{\langle x_4 \rangle}{\langle x_2 \rangle^2} = \frac{\left(\int_{-\infty}^{\infty} |\psi(x,z)|^2 x^4 dx\right)\left(\int_{-\infty}^{\infty} |\psi(x,z)|^2 dx\right)}{\left(\int_{-\infty}^{\infty} |\psi(x,z)|^2 x^2 dx\right)^2} \quad (12)$$

M^2 increases by increasing the mode number, while the kurtosis number decreases by increasing the mode number. The M^2 and the *k*-factor of the constructed Gaussian beam produced by the modulator unit are 1.2 and 2.8, respectively.

These values confirm a marked improvement compared with the original multimode beam. This is further confirmed by comparison of the light sheets produced by the 2 different beams generated with and without the beam modulator. We validated our model by using other multimode lasers. The method to generate a reconstructed Gaussian beam from multimode lasers that is described in this paper may help to decrease the price of ultramicroscopy systems, making them more affordable for scientists needing lasers with different wavelengths.

AUTHOR BIOGRAPHIES

Please see Supporting Information online.

ORCID

Saiedeh Saghafi http://orcid.org/0000-0002-7598-541X
Klaus Becker http://orcid.org/0000-0002-2406-0476

REFERENCES

[1] J. M. Cowley, *Diffraction Physics*, Elsevier Science, Amsterdam **1995**.
[2] R. Kant, *J. Mod. Opt.* **1993**, *40*(11), 2293.
[3] J. W. Goodman, *Introduction to Fourier Optics*, Roberts and Company Publishers, Englewood, Colorado **2005**.
[4] A. E. Siegman, *Lasers*, University Science Books, Sausalito, California, Vol. *37*, Mill Val. CA **1986**, p. 462.
[5] H. Laabs, C. Gao, H. Weber, N. Kugler, C. M. Zhao, *Transformation of Hermite-Gaussian beams into complex Hermite-Gaussian and Laguerre-Gaussian beams*, SPIE conference on laser resonators, San Jose, California Vol. *3611* **1999**, p. 258.
[6] F. Gori, *Opt. Commun.* **1994**, *107*(5), 335.
[7] C. J. R. Sheppard, S. Saghafi, *Opt. Commun.* **1996**, *132*(1–2), 144.
[8] H.-U. Dodt, S. Saghafi, K. Becker, N. Jährling, C. Hahn, M. Pende, M. Wanis, A. Niendorf, *Neurophotonics* **2015**, *2*(4), 41407.
[9] G. Feng, R. H. Mellor, M. Bernstein, C. Keller-Peck, Q. T. Nguyen, M. Wallace, J. M. Nerbonne, J. W. Lichtman, J. R. Sanes, *Neuron*, *28*(1), 41.
[10] D. R. Jones, C. D. Perttunen, B. E. Stuckman, *J. Optim. Theory Appl.* **1993**, *79*(1), 157.
[11] S. Saghafi, K. Becker, C. Hahn, H. U. Dodt, *J. Biophotonics* **2014**, *7*(1–2), 117.
[12] S. Saghafi, C. J. R. Sheppard, *Opt. Commun.* **1998**, *153*(4), 207.
[13] S. Saghafi, M. J. Withford, Z. Ghoranneviss, *Can. J. Phys.* **2006**, *84*-(MARCH), 223.
[14] H.-U. Dodt, U. Leischner, A. Schierloh, N. Jährling, C. P. Mauch, K. Deininger, J. M. Deussing, M. Eder, W. Zieglgänsberger, K. Becker, *Nat. Methods* **2007**, *4*(4), 331.

SUPPORTING INFORMATION

Additional Supporting Information may be found online in the supporting information tab for this article.

Appendix S1. Gaussian beam mode in angular spectrum modal analysis.

Video S1. Multimode and monomode.

Video S2. Multi-mode and mono-mode beams.

Video S3. Constructed Gaussian beam and monomode beam.

Video S4. VID-20170717-WA0005.

Video S5. Cancer movie.

How to cite this article: Saghafi S, Haghi-Danaloo N, Becker K, et al. Reshaping a multimode laser beam into a constructed Gaussian beam for generating a thin light sheet. *J. Biophotonics*. 2018; e201700213. https://doi.org/10.1002/jbio.201700213